African Multidisciplinary
Journal of Sciences and Artificial Intelligence

ISSN : 1595-7969

Index: Harvard, Boston, Sydney University, Dimensions, Lens, ResearchGet Scilit, Semantic, Google Scholar, Base etc

https://doi.org/10.58578/AMJSAI.v3i3.11642

Inverted Bilayered Opal Photoanodes for Dye Sensitised Solar Cells

E. A. Kamba, E. A. Yerima, E. B. AttahDaniel
Federal University, Wukari, Taraba State, Nigeria
emma@fuwukari.edu.ng

Article Info:

Submitted:	Revised:	Accepted:	Published:
Jun 19, 2026	Jul 17, 2026	Jul 29, 2026	Aug 3, 2026

Abstract

Developing efficient photoanode materials remains a major challenge in improving the performance of dye-sensitized solar cells (DSSCs). This study aims to fabricate and evaluate a bilayer photoanode comprising potassium titanate ($K_2Ti_4O_9$) nanobelts coupled with a zinc oxide (ZnO) inverse-opal structure and to investigate the effects of electrolyte cation identity and concentration on DSSC performance. $K_2Ti_4O_9$ nanobelts were synthesized through a solid-state reaction between potassium carbonate (K_2CO_3) and titanium dioxide (TiO_2) and subsequently integrated with the ZnO inverse-opal layer. Photocurrent–voltage measurements were conducted using a two-electrode DSSC configuration containing an I_3^-/I^- redox electrolyte. The devices were illuminated using a 300 W xenon arc lamp equipped with an AM 1.5G filter at an intensity of 100 mW cm^{-2}. The findings show that the ZnO inverse-opal/$K_2Ti_4O_9$ bilayer system achieved a photoelectric conversion efficiency of 1.19%, exceeding the 1.04% efficiency obtained using the single $K_2Ti_4O_9$ system. This improvement indicates that the ZnO inverse-opal layer contributes substantially to device performance by functioning as a photonic-crystal underlayer. The study demonstrates the potential of integrating ZnO inverse-opal structures with $K_2Ti_4O_9$ nanobelts to

AMJSAI Journal is licensed under a Creative Commons Attribution-NonCommercial-ShareAlike 4.0 International License

enhance DSSC photoanode performance and provides a basis for developing bilayered photonic architectures for solar-energy conversion.

Keywords: Dye-Sensitized Solar Cells; Photonic Crystal; Potassium Titanate Nanobelts; Photoanode; Zinc Oxide Inverse Opal

Introduction

In an attempt to enhance DSSC efficiency, the use of bilayered heterostructures which consists of two different nanostructures as photoanodes [1], is quite promising. This is because the high surface area of the macroporous inverse opal nanostructures enhances dye absorption and infiltration of electrolyte [2,3]. Similarly, the formation of hierarchical porosity introduced by two inverse opal layers may be beneficial through an increased surface area which enhances mass transport with better charge separation, consequently acting as another photoenhancement factor [4].

In this study, a monolayer ZnO inverse opal coupled with another nanostructure, potassium titanate ($K_2Ti_4O_9$) nanobelts have been investigated. The reasons for choice of potassium titanate nanobelts as coupling agent are highlighted as follows: 1) due to its wide band gap (3.53 eV); it may contribute to enhanced charge separation as well as transfer properties of the photoanode, 2) due to the formation of interfaces, composites of titanates and other metal oxide nanostructures have exhibited enhanced light harvesting properties [5], 3) in this work, the average length of titanate nanobelts used is in the scale of several tens of micrometers. As such, they could cover the top of the underlying ZnO inverse opal film resulting in the introduction of more surface area for enhanced electrolyte infiltration, effective dye sensitization as well as charge collection [6]. Moreover, $K_2Ti_4O_9$ forms the center of this work in studying the effects of the underlying macroporous monolayer ZnO inverse opal in enhancing light harvesting for better energy conversion.

Material and Methods

Photoanode samples preparation

The synthesis of $K_2Ti_4O_9$ nanobelts was performed according to the solid-state method reported by Allen et al [7]. K_2CO_3 and TiO_2 (P25) were mixed and ground together in a 1:3 molar ratio using a mortar and a pestle. The mixture was then annealed at 960°C for 10 h

at 15°C/min ramping rate. For photoanode preparation, $K_2Ti_4O_9$ nanobelts paste was first prepared as follows: Polyvinyl alcohol (PVA) water solution (30%, 3g) was dissolved in a mixed solvent of water (9.0 ml) and ethanol (12.5 ml). 2.2 g sample of $K_2Ti_4O_9$ nanobelts was then added to create the nanobelts suspension. After the suspension was dispersed, two samples were made; first, a layer of $K_2Ti_4O_9$ nanobelts paste was deposited onto the previously made monolayer ZnO inverse opal on the FTO substrate following doctor blade technique. A reference photoanode was prepared by directly depositing onto the FTO glass substrate a layer of $K_2Ti_4O_9$ nanobelts paste, using the doctor blade technique. In order to control the thickness, a layer of double sided cellophane was used. The thickness of both films above the FTO surface was measured to be approximately 25 microns. The photoanode samples were dried for 2 h, and then calcined at 550°C with a ramping rate of 3°C/min for 2 h to remove the organic residues from the pastes.

To study the effects of cation identity as well as concentration in the electrolyte media of a DSSC, P25 sample on the FTO glass was used as the photoanode nanomaterial. This was prepared by making a P25 paste using similar procedure as in making of $K_2Ti_4O_9$ nanobelts paste, but by replacing $K_2Ti_4O_9$ with 1.62g P25. Again doctor blade technique was applied to deposit the P25 paste onto the FTO substrate, achieving film thickness of about 25 microns above the FTO surface. This was then dried and calcined at 550°C for 2 h. In addition to the removal of organic residues from the P25 paste, calcination at this temperature was also beneficial for improving the crystallinity of the P25 sample.

Prior to dye sensitization, all the as-sensitized films deposited on the FTO glass substrates were heated at 85°C for 30 minutes to enhance dye adhesion. The photoanode samples were then immersed in a dye solution, N719 dye (0.3 mM) in ethanol for 24 hours. To create the counter electrodes (photocathodes) a clean FTO glass substrate was coated with a drop of 0.5 mM chloroplatinic acid (H_2PtCl_6) in ethanol, dried and calcined at 400°C for 20 minutes. This gave a very thin layer of Pt about 100 nm thick deposited on the FTO substrate. A sandwich type cell comprising each photoanode and a counter electrode was assembled in pairs. In each pair, the active sides of the photoanode and counter electrode faced each other. A spacer, consisting of 2 layers of double sided tape about 50 microns, was used to control the gap between the two electrodes. The assembled electrodes were then sealed using UV-sensitive glue (Loctite 358) leaving the top side of the cells unsealed for electrolyte infiltration. To dry the seals, the cells were placed under a UV light source for 45 min. An active area of 1 cm^2 was maintained for all the cells. This was followed by the introduction of a few drops of

I_3^- / I^- electrolyte solution consisting of 0.6M 1-methyl-3-n-propylimidazolium iodide (PMII), 0.5 M 4-tert-butylpyridine (TBP), 0.05 M iodine (I2) and 0.1M lithium iodide (LiI) in dry acetonitrile, from the unsealed sides of the cells into the gap between the working and counter electrodes. Infiltration took place through capillary forces, wetting the entire active areas of the cells ultimately yielding the finished DSSCs.

Photovoltaic Characterization

In order to measure the photocurrent-voltage (*I–V*) characteristics of the DSSCs in a two electrode system, an eDAQ potentiostat, scanning from a negative bias of -1200 mV to a positive bias of 200 mV was used.

Artificial solar light generated by 300 W xenon lamp and AM 1.5G filter was used for all the measurements. The intensity of the lamp was adjusted to a power density of 100 mW/cm^2, corresponding to 1 sun.

Results and Discussion

Morphology

Figure 1 shows the morphologies the various materials used for the study beginning from that of P25 (Figure 1a), which is an aggregate crystalline TiO_2 nanoparticles. $K_2Ti_4O_9$ nanobelts were coupled with a monolayer ZnO inverse opal and utilized as photoanode in a DSSC in order to investigate the effects of the underlying inverse opal with the aim of enhancing the photoefficiency of the cell. A layer of $K_2Ti_4O_9$ nanobelts deposited on a FTO glass (film thickness above the substrate ~25 microns) is shown in Figure 1b while a monolayer ZnO inverse opal templating on a FTO glass substrate (film thickness ~410 nm) is seen in Figure 1c. Figure 1d shows a monolayer ZnO inverse opal-$K_2Ti_4O_9$ nanobelt composite on a FTO glass.

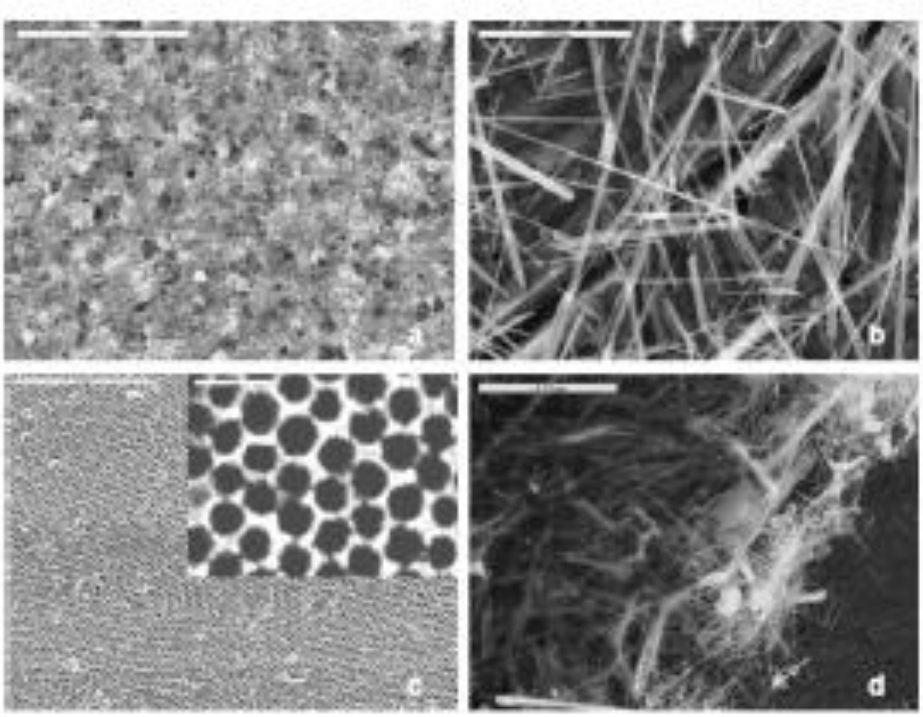


Figure 1: Thin film SEM images of (a) P25, (b) $K_2Ti_4O_9$ nanobelts, (c) monolayer ZnO inverse opal and (d) monolayer ZnO inverse opal-$K_2Ti_4O_9$ nanobelts composite. FTO glass substrates were used for all samples. Scale bars: (a) 50µm, (b) 20µm, (c) 10µm, (c inset) 1µm and (d) 100µm.

The $K_2Ti_4O_9$ nanobelts were deposited directly onto the underlying inverse opal thin film adopting the doctor blade technique. As determined *via* the Scherrer equation, the average crystallite size is 20 nm. Various thicknesses of the nanobelts ranging from 60 nm to 170 nm were measured. Also, various lengths between 1.5 to 6 microns were recorded. From the SEM image in Figure 1c, a clear highly ordered and crack-free monolayer ZnO inverse opal can be seen, which was used as a photonic crystal under-layer in combination with $K_2Ti_4O_9$ nanobelts (Figure 1d).

Crystal Property Characterisation

As observed from XRD data, the $K_2Ti_4O_9$ nanobelt structure in Figure 1b is highly crystalline. In order of sequence of formation of the crystal structures of the other nanomaterial used as photoanode in DSSC experiments in this work, namely monolayer ZnO inverse opal-$K_2Ti_4O_9$ nanobelt composite is presented in Figure 2. The green spectrum is the XRD pattern for $K_2Ti_4O_9$ nanobelts; the red spectrum is the monolayer ZnO inverse opal and the blue spectrum is the monolayer ZnO inverse opal-$K_2Ti_4O_9$ nanobelts composite.

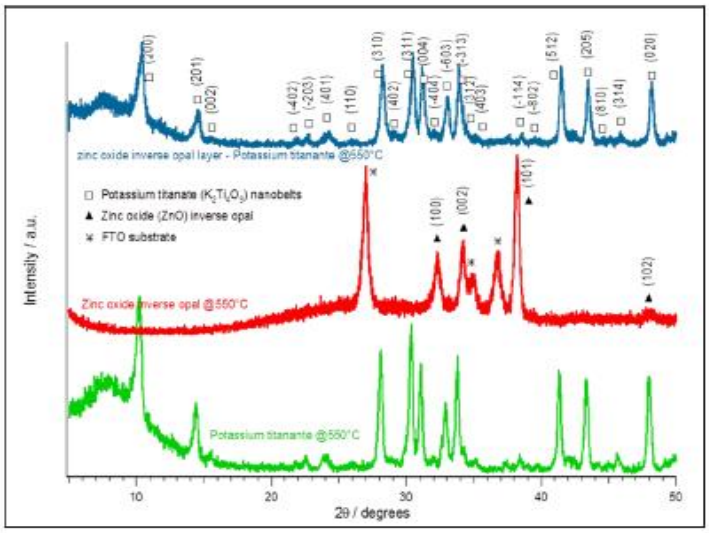


Figure 2: XRD patterns for $K_2Ti_4O_9$ nanobelts (green spectrum), ZnO inverse opal (red spectrum) and monolayer ZnO inverse opal-$K_2Ti_4O_9$ nanobelts composite (blue spectrum) all produced at 550°C.

The diffraction peaks of the titanate sample (green spectrum) correspond well with that reported in the literature [7], indicating the crystalline phase of $K_2Ti_4O_9$. These sharp and highly intense peaks are indexed to the JCPDS reference card number (00-032-0861), indicating high crystallinity of the sample. The $K_2Ti_4O_9$ crystallite size, perpendicular to the (200) plane was determined by the Debye-Scherrer equation to be 25 nm. Xiong *et al* [8], reported that the crystal phase of $K_2Ti_4O_9$ possesses a layered structure, which consists of ribbons of edge and corner shared TiO_6 octahedral units and separated by K ions.

The diffraction peaks of the ZnO inverse opal sample (red spectrum) were indexed to a hexagonal wurtzite phase of ZnO (JCPDS reference no. 01-075-1526). The peaks corresponding to the underlying FTO glass substrate are labelled with stars.

Upon introduction of the monolayer ZnO under-layer (blue spectrum), only resolved diffraction peaks for the $K_2Ti_4O_9$ nanobelts in the composite were observed. No characteristic change from its original spectrum (green spectrum) was observed. The very low intensities of the diffraction peaks of the underlying monolayer ZnO inverse may be attributed to its very thin nature (about 410 nm thick) in comparison with the thick layer of $K_2Ti_4O_9$ nanobelts (about 25 microns thick). Hence, the XRD patterns for the underlying inverse opal thin film could not be detected.

DSSC Performance Test

$K_2Ti_4O_9$ nanobelts coupled monolayer ZnO inverse opal were utilized for as photoanode in DSSC in order to study the effects of the underlying inverse opal on the cell performance. For reference, a pristine sample of $K_2Ti_4O_9$ nanobelt was used without the presence of the underlying monolayer inverse opal. The *I-V* characteristics and photo conversion efficiency are presented in Figures 3(a) and 3(b) respectively. The curves for the as-assembled cells with monolayer ZnO inverse opal-$K_2Ti_4O_9$ nanobelt composite is given by the blue curves while the $K_2Ti_4O_9$ nanobelts stand alone is shown by red curves, which were used as photo anodes under 100mWcm^{-2} irradiation.

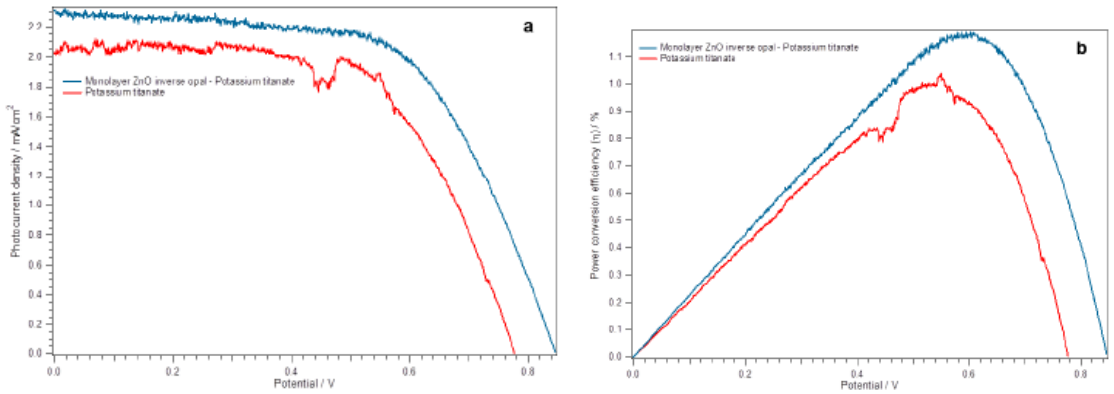


Figure 3: (a) *I-V* characteristics and (b) photo efficiencies of DSSCs assembled with $K_2Ti_4O_9$ nanobelts only (red curve) and monolayer ZnO inverse opal-$K_2Ti_4O_9$ nanobelts composite (blue curve) as photoanodes.

Table 1 gives the summary of the corresponding photovoltaic parameters of the two cells. From this Table, it is clear that the main parameters, *JSC*, *VOC* and photo-conversion efficiency (η%), improved when the $K_2Ti_4O_9$ nanobelt structure was coupled with a thin underlying monolayer ZnO inverse opal in comparison without. These observations may suggest the role of the underlying inverse opal layer in harnessing light, hence the overall improved performance.

Table 1: Photovoltaic Parameters of DSSCs assembled with $K_2Ti_4O_9$ nanobelts and monolayer ZnO inverse opal-$K_2Ti_4O_9$ nanobelts composite, as photoanodes.

Photoanodes	JSC/mAcm^{-2}	VOC/V	η%	FF
$K_2Ti_4O_9$ nanobelts	2.02	0.777	1.04	0.660
Monolayer ZnO inverse opal-$K_2Ti_4O_9$ nanobelt	2.31	0.845	1.19	0.611

As observed from the XRD patterns in Figure 2, there are neither new detectable peaks nor any changes in the characteristics of the $K_2Ti_4O_9$ nanobelts. This indicates that there are no new structures formed at the interface between the two layers. Coupling an inverse opal

layer of TiO_2 as a photonic crystal layer to a non-structured layer of TiO_2 thin film in a DSSC has being demonstrated as vital in DSSC. Mallouk and his colleagues [9,10], reported that efficiency was enhancement by using the inverse opal as a top layer on a TiO_2 based DSSC while irradiating from the anode side. They suggested that the enhanced efficiency achieved may be attributed to the TiO_2 inverse opal layer acting as photonic crystal mirror in the bilayer architecture, consequently creating localized states in the non-structured surface layer of TiO_2 thin film. In our context, the creation of partially localized resonant modes in the $K_2Ti_4O_9$ top layer via the underlying inverse opal may also be another photonic enhancement effect arising in this bilayer architecture as ZnO inverse opal may act as a reflective mirror [11,12]. Therefore, the underlying ZnO inverse opal may act as a photonic crystal material in the inverse opal-$K_2Ti_4O_9$ nanobelts composite for enhanced light harvesting over a broad wavelength. Moreover, the ZnO inverse opal, also has another interesting property; a high surface area with interconnected macroporous skeleton. This property may be beneficial with respect to higher dye sensitizer loading as well as faster electron transport. The highly porous structure may also provide a platform for better electrolyte diffusion in the inverse opal-$K_2Ti_4O_9$ nanobelt composite system. It is also worthy of note that shorter diffusion distance between the photoanode/electrolyte may reduce charge recombination at the interface.

Conclusion

The importance of cation in the electrolyte media was investigated in this work. Using ZnO inverse opal as a photonic crystal material enhances the overall efficiency of $K_2Ti_4O_9$ nanobelt based cell, which is possibly achieved by enhancing localization and scattering of light due first, to the photonic crystal mirror effect and secondly, through creation of resonant modes in the bilayer architecture. The highly interconnected porous inverse opal can enhance internal surface area and also contribute to enhanced light harvesting due to a shorter diffusion length ultimately resulting in better dye adsorption. This indicates that engineering a suitable multilayer heterojunction of layer-by-layer inverse opal nanostructure with alternative p-n layers may improve the efficiencies of DSSCs. Nevertheless, establishing suitable semiconductors, which can align their band edges together to form junctions, may pose a challenge in the future.

References

1. Zhang, Q., & Cao, G. (2011). Nanostructured photoelectrodes for dye-sensitized solar cells. *Nano Today, 6*(1), 91–109. https://doi.org/10.1016/j.nantod.2010.12.007
2. Pan, K., Dong, Y. Z., Zhou, W., Pan, Q. J., Xie, Y., Xie, T. F., Tian, G. H., & Wang, G. F. (2013). Facile fabrication of hierarchical TiO_2 nanobelt/ZnO nanorod heterogeneous nanostructure: An efficient photoanode for water splitting. *ACS Applied Materials & Interfaces, 5*(17), 8314–8320. https://doi.org/10.1021/am402154k
3. Li, H., Zhou, Y., Lv, C. X., & Dang, M. M. (2011). Templated synthesis of ordered porous TiO_2 films and their application in dye-sensitized solar cell. *Materials Letters, 65*(12), 1808–1810. https://doi.org/10.1016/j.matlet.2011.03.044
4. Choudhary, S., Upadhyay, S., Kumar, P., Singh, N., Satsangi, V. R., Shrivastav, R., & Dass, S. (2012). Nanostructured bilayered thin films in photoelectrochemical water splitting—A review. *International Journal of Hydrogen Energy, 37*(24), 18713–18730. https://doi.org/10.1016/j.ijhydene.2012.10.028
5. Townsend, T. K., Browning, N. D., & Osterloh, F. E. (2012). Nanoscale strontium titanate photocatalysts for overall water splitting. *ACS Nano, 6*(8), 7420–7426. https://doi.org/10.1021/nn302647u
6. Chen, Y., Tang, Z. F., & Chen, Z. G. (2013). Fabrication of three-dimensionally ordered macroporous TiO_2 films with enhanced photovoltaic conversion efficiency. *Journal of Inorganic and Organometallic Polymers and Materials, 23*(4), 839–845. https://doi.org/10.1007/s10904-013-9850-9
7. Allen, M. R., Thibert, A., Sabio, E. M., Browning, N. D., Larsen, D. S., & Osterloh, F. E. (2010). Evolution of physical and photocatalytic properties in the layered titanates $A_2Ti_4O_9$ (A = K, H) and in nanosheets derived by chemical exfoliation. *Chemistry of Materials, 22*(3), 1220–1228. https://doi.org/10.1021/cm902695r
8. Xiong, Z. G., & Zhao, X. S. (2012). Nitrogen-doped titanate-anatase core–shell nanobelts with exposed {101} anatase facets and enhanced visible light photocatalytic activity. *Journal of the American Chemical Society, 134*(13), 5754–5757. https://doi.org/10.1021/ja300730c
9. Lee, S.-H. A., Abrams, N. M., Hoertz, P. G., Barber, G. D., Halaoui, L. I., & Mallouk, T. E. (2008). Coupling of titania inverse opals to nanocrystalline titania layers in dye-sensitized solar cells. *The Journal of Physical Chemistry B, 112*(46), 14415–14421. https://doi.org/10.1021/jp802692u
10. Abrams, N. M., Halaoui, L. I., & Mallouk, T. E. (2004). Increased efficiency of dye-sensitized solar cells through the localization of light. *ACS National Meeting Book of Abstracts, 228*(1), 577.
11. Paquet, C., & Kumacheva, E. (2008). Nanostructured polymers for photonics. *Materials Today, 11*(4), 48–56. https://doi.org/10.1016/S1369-7021(08)70056-7
12. Tański, T., Jarka, P., Szindler, M., Drygała, A., Matysiak, W., & Libera, M. (2019). Study of dye-sensitized solar cells photoelectrodes consisting of nanostructures. *Applied Surface Science, 491*, 807–813. https://doi.org/10.1016/j.apsusc.2019.04.274
13. Zheng, H., Shah, S. K., Abbas, M., Ly, I., Rivera, T., Almeida, R. M., Hirsch, L., Toupance, T., & Ravaine, S. (2016). Efficiency enhancement in solid state dye-sensitized solar cells by including inverse opals with controlled layer thicknesses.

Photonics and Nanostructures—Fundamentals and Applications, 21, 13–18. https://doi.org/10.1016/j.photonics.2016.05.001

14. Karuturi, S. K., Cheng, C., Liu, L., Su, L. T., Fan, H. J., & Tok, A. I. Y. (2012). Inverse opals coupled with nanowires as photoelectrochemical anode. *Nano Energy, 1*(2), 322–327. https://doi.org/10.1016/j.nanoen.2012.01.001